JACS
JOURNAL OF THE AMERICAN CHEMICAL SOCIETY

Communication

pubs.acs.org/JACS

Synthesis and Facet-Dependent Photoreactivity of BiOCl Single-Crystalline Nanosheets

Jing Jiang, Kun Zhao, Xiaoyi Xiao, and Lizhi Zhang*

Key Laboratory of Pesticide & Chemical Biology of the Ministry of Education, College of Chemistry, Central China Normal University, Wuhan 430079, P. R. China

Supporting Information

ABSTRACT: BiOCl single-crystalline nanosheets with exposed {001} and {010} facets were selectively synthesized via a facile hydrothermal route. The resulting BiOCl single-crystalline nanosheets with exposed {001} facets exhibited higher activity for direct semiconductor photoexcitation pollutant degradation under UV light, but the counterpart with exposed {010} facets possessed superior activity for indirect dye photosensitization degradation under visible light.

Surface properties are crucial to the physical and chemical performance of a single-crystalline material. Usually, different facets of a single-crystalline material possess different geometric and electronic structures, thus endowing them with distinctive properties.[1−4] Recently, considerable attention has been paid to the facet-controlled fabrication of single-crystalline semiconductors with well-defined morphologies because of their facet-dependent photocatalytic, photoelectric, and other surface-related properties.[5−8] Especially, surface properties are vital to a semiconductor's photocatalytic performance, which sensitively depends on its exposed surfaces with distinct crystal facets.[9−14] For example, recent progress made by Lu and co-workers on the synthesis of anatase single crystals with highly reactive {001} facets have paved a new way for the enhancement of photocatalytic performance.[15−17] They demonstrated theoretically and experimentally that the {001} facets of anatase are much more reactive than the thermodynamically more stable {101} facets. Undoubtedly, facet engineering not only is an exciting direction to pursue for highly active new-generation photocatalysts but also offers opportunities to investigate the relationship between the surface properties and the photocatalytic properties.

In this communication, we first report on the facet-controllable synthesis of BiOCl single-crystalline nanosheets (BOC SCNSs) with exposed {001} and {010} facets and their facet-dependent photoreactivity for photodegradation of methyl orange (MO) via direct semiconductor photoexcitation under UV light and indirect dye photosensitization under visible light. Structural insights into the interesting differences are provided on the basis of detailed experimental results.

BOC SCNSs were synthesized by reacting $Bi(NO_3)_3{\cdot}5H_2O$ and KCl in distilled water via a facile hydrothermal route at 160 °C. The facet control was realized by adjusting the pH of the solution by addition of NaOH. The samples obtained in the absence and presence of NaOH were denoted as BOC-001 and BOC-010, respectively. Scanning electron microscopy (SEM) examination revealed that the BOC-001 sample consisted of large-scale sheet-shaped structures with widths of 1−3 μm and thicknesses of 80−200 nm (Figure S1 in the Supporting Information). Transmission electron microscopy (TEM) images of an individual nanosheet (Figure 1a and Figure S2 further confirmed its sheet-shaped structure. The corresponding selected-area electron diffraction (SAED) pattern (Figure 1b) indicated the single-crystalline characteristic of the BOC-001 sample. The angle labeled in the SAED pattern is 45°, which is in agreement with the theoretical value of the angle between the (110) and (200) planes. The set of diffraction spots can be indexed as the [001] zone axis of tetragonal BiOCl. High-resolution TEM (HRTEM) (Figure 1c) revealed the highly crystalline nature of the nanosheets. The clear lattice fringes with an interplanar lattice spacing of 0.275 nm correspond to the (110) atomic planes. On the basis of the above results and the symmetries of tetragonal BiOCl, the

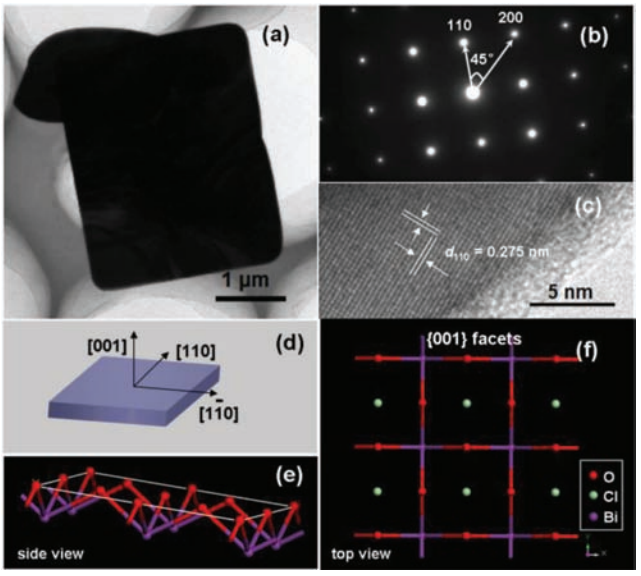

Figure 1. (a) TEM image, (b) SAED pattern, and (c) HRTEM image of the BOC-001 SCNSs. (d) Schematic illustration of the crystal orientation of the nanosheet. (e, f) Atomic structure of the {001} facets: (e) side view; (f) top view.

Received: November 8, 2011
Published: March 1, 2012

   dx.doi.org/10.1021/ja210484t | J. Am. Chem. Soc. 2012, 134, 4473−4476

bottom and top surfaces of the BOC-001 sample are identified as {001} facets, while the four lateral surfaces are {110} facets (Figure 1d). The percentage of {001} facets was estimated from the geometric calculation to be ca. 80% for the BOC-001 sample. The atomic structure of the {001} facets is characterized by the high density of oxygen atoms (Figure 1e,f).

The electron microscopy observations showed that the BOC-010 product also presents well-defined sheet-shaped structures (Figure 2a and Figures S3–S5). The width and thickness of the

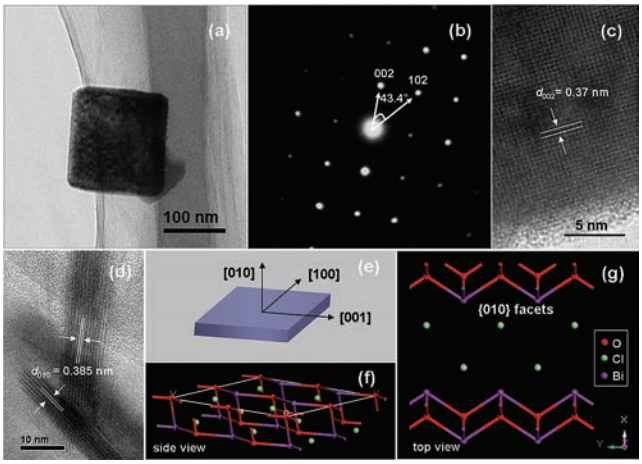

Figure 2. (a) TEM image, (b) SAED pattern, and (c, d) HRTEM images of the BOC-010 SCNSs. (e) Schematic illustration of the crystal orientation of the nanosheet. (f, g) Atomic structure of the {010} facets: (f) side view; (g) top view.

sheets were estimated to be 150–600 and 10–60 nm, respectively. The corresponding SAED pattern, indexed as the [010] zone, displays (002) and (102) planes with an interfacial angle of 43.4° (Figure 2b), which is identical to the theoretical value. A typical HRTEM image of a BOC-010 nanosheet (Figure 2c) shows clear and continuous lattice fringes. The (002) atomic planes with a lattice spacing of 0.37 nm can be obviously observed. Furthermore, the HRTEM image of vertical nanosheets (Figure 2d) shows the lattice fringe spacing of 0.385 nm, which is assigned to the (010) planes of BiOCl. Hence, these BOC SCNSs are enclosed by dominant {010} facets (Figure 2e). The percentage of {010} facets exposed on the surface of the BOC-010 SCNSs was estimated to be ca. 73%. The atomic structure of the {010} facets (Figure 2f,g) indicates its open channel feature.

As evidenced by X-ray diffraction (XRD) characterization (Figure S6), the intensity ratios of the (002) and (200) peaks were 5.88 and 1.07 for BOC-001 and BOC-010, respectively. This difference in the intensity ratios reflects the difference between the surfaces of the two samples, which is in good agreement with the HRTEM and SAED results. UV–vis diffuse-reflectance spectroscopy (DRS) (Figure S7) showed that two BOC SCNSs samples have very close absorption edges in the UV region and very similar band-gap energies, which were estimated to be 3.31 and 3.29 eV, respectively.

The success in controlling the facet exposure for the BOC SCNSs allowed us to investigate their facet-dependent photocatalytic performance systematically. It is well-established that the photocatalytic degradation of dyes on semiconductors can originate from two kinds of processes, namely, direct semiconductor photoexcitation and indirect dye photosensitization. To this end, the photocatalytic performances of the BOC SCNSs were evaluated using MO as the probe molecule under UV (λ = 254 nm) or visible (λ > 420 nm) light irradiation, respectively. We first investigated the photocatalytic abilities of the BOC SCNSs to degrade MO under UV light. We found MO was slightly self-degraded (13% in 45 min) under UV light in the absence of photocatalyst (Figure S8). However, the presence of the BOC SCNSs resulted in more obvious degradation of MO under UV light. After UV light irradiation for 45 min, the photodegradation efficiencies of MO over BOC-001 and BOC-010 were ca. 99% and 59%, respectively. BOC-001 exhibits a higher apparent reaction rate constant (k) than BOC-010 (Figure 3). Since BOC-001

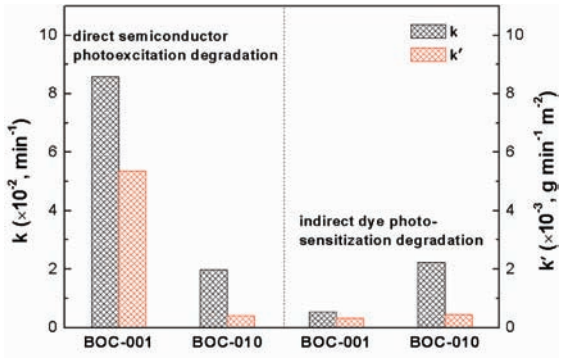

Figure 3. Comparison of the apparent reaction rate constants for photocatalytic degradation of MO over the BOC SCNSs under (left) UV (λ = 254 nm) and (right) visible-light (λ > 420 nm) irradiation.

has a smaller specific surface area than BOC-010 (Figure S9), its apparent reaction rate constant normalized by the surface area (k') is also higher than that of BOC-010 (Figure 3), suggesting that the direct semiconductor photocatalysis of the BOC SCNSs is related to surface structure rather than surface area.

Under visible-light irradiation, the photodegradation of MO would take place via an indirect dye photosensitization process, as these large-band-gap BOC SCNSs could not be excited under visible light (Figure S10). We further studied the photocatalytic degradation of MO over the BOC SCNSs under visible-light irradiation to gain insight into the surface-related photosensitization process. Interestingly, similar to the direct semiconductor photocatalysis, the dye photosensitization process also depends on the photocatalyst's surface, although the MO photodegradation over BOC SCNSs must be initiated with the help of MO photoexcitation. The MO degradation efficiencies over BOC-001 and BOC-010 were ca. 10% and 33%, respectively, under visible-light irradiation for 180 min (Figure S10b). Obviously, BOC-010 exhibits a much higher photosensitization degradation activity than BOC-001, in contrast to the case of the semiconductor photocatalysis process. This suggests that BOC SCNSs with different exposed facets possess different light-dependent photocatalytic properties. More importantly, the k value for BOC-010 significantly decreased upon normalization by the surface area, and the normalized k' values of BOC-010 and BOC-001 became close (Figure 3), clearly suggesting that the photosensitization degradation process is strongly associated with the surface area.

The stability of the BOC SCNSs during photocatalytic reaction was further explored by recycling tests and XRD measurements (Figures S6 and S11). No significant change in the photocatalytic activity and crystalline structure was

dx.doi.org/10.1021/ja210484t | J. Am. Chem. Soc. 2012, 134, 4473–4476

observed after three cycles, indicating that the BOC SCNSs were very stable during photocatalysis.

To understand the origin of the facet-dependent photoreactivity of the BOC SCNSs, we carefully examined the process of MO adsorption over BOC-001 and BOC-010. The results (Figure S12) revealed that the BOC-010 possesses a higher MO adsorption capacity than BOC-001, which might be associated with the active sites on the surface of the BOC SCNSs. The adsorption capacities of MO were estimated to be 0.2 and 0.9 mg g^{-1} for BOC-001 and BOC-010, respectively. The aforementioned structural characteristics reveal that the BOC-001 surface atomic structure contains terminal oxygen atoms, and their (001) surfaces are expected to be more negatively charged than those of the BOC-010. The repulsive interaction between the negatively charged (001) surface and the anionic MO dye is responsible for the poor dye adsorption ability of BOC-001. On the other hand, the surface atomic structure of BOC-010 presents the open channel characteristic, offering more active sites and larger accommodation space for the MO adsorption. For BOC-010, the adsorption capacity normalized by the surface area (0.19 mg m^{-2}) was significantly higher than that of BOC-001 (0.12 mg m^{-2}), confirming that the higher adsorption capacity of BOC-010 could be attributed not only to the surface area factor but also to its open channel characteristic.

BiOCl has a unique layered structure (Figure 4a), characterized by $[Bi_2O_2]$ slabs interleaved with double slabs

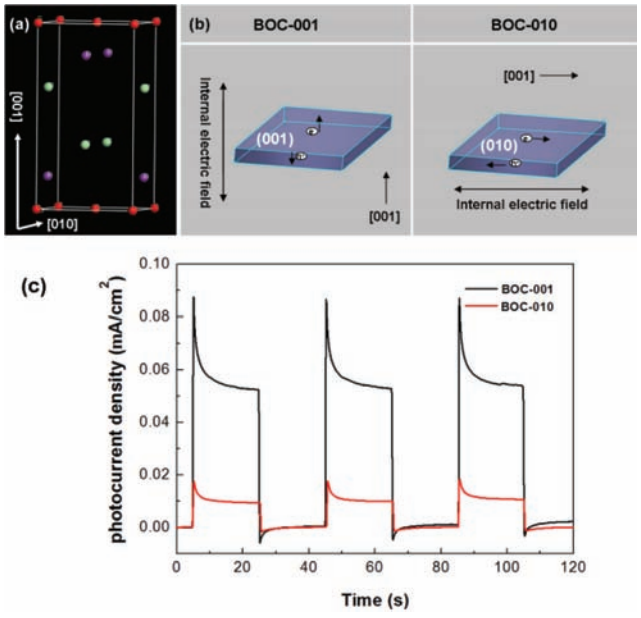

Figure 4. (a) Crystal structure of BiOCl. (b) Model showing the direction of the internal electric field in each of the BOC SCNSs. (c) Photocurrent responses of the BOC SCNSs in 0.5 M Na_2SO_4 aqueous solutions under UV–vis irradiation.

of halogen atoms. This would induce the presence of internal static electric fields perpendicular to the $[Bi_2O_2]$ slabs and halogen anionic slabs in BiOCl,[18] enabling the effective separation of the photoinduced electron–hole pairs along the [001] direction. As schematically illustrated in Figure 4b, the self-induced internal electric fields are perpendicular to the nanosheets of BOC-001 but parallel to those of BOC-010. Therefore, the charge separation and transfer assisted by the internal electric fields are more favorable in BOC-001, with a shorter diffusion distance of photoinduced charge carriers than that in the BOC-010, as confirmed by the transient photocurrent responses of the two BOC SCNS films (Figure 4c and Figure S13). Both electrodes were prompt in generating photocurrent with a reproducible response to on/off cycles, but the BOC-001 film electrode exhibited a higher photocurrent than the BOC-010 film electrode, indicating the more efficient photoinduced charge separation and transfer in BOC-001.

Photoluminescence (PL) emission is a common and useful technique to survey the separation efficiency of the photogenerated charge carriers in a semiconductor because the recombination of excited electrons and holes gives rise to the PL emission signal.[19] A lower PL intensity is generally indicative of a lower recombination rate. As shown in Figure S14, the PL spectra of the BOC SCNSs display emission peaks in the 340–450 nm range under the excitation at 320 nm.[20] The weaker PL intensity of BOC-001 confirms its better efficiency of separation of photogenerated electron–hole pairs.

On the basis of the above results, we can analyze the origin of the facet-dependent photreactivity of the BOC SCNSs during direct semiconductor photoexcitation and indirect dye photosensitization MO degradation processes. The semiconductor photocatalysis process generally involves semiconductor photoexcitation, separation of the photoelectrons and photoholes, bulk diffusion, surface transfer of the photoinduced charge carriers, generation of active species, and pollutant degradation,[21,22] which are cooperatively determined by the electronic structure and surface properties. In comparison with BOC-010, although BOC-001 has a very similar absorption edge and smaller surface area, it exhibits higher photoreactivity during the direct semiconductor photoexcitation process, which should be attributed to surface structure rather than electronic structure. Meanwhile, the self-induced internal electric fields could induce more efficient photoinduced charge separation and transfer along the [001] direction in the nanosheets than along the [010] direction, as shown in Figure 4, which can inhibit the recombination of photogenerated electron–hole pairs to increase the photocatalytic degradation of MO. Therefore, a cooperative effect between the surface properties and suitable internal electric fields might account for the higher photoreactivity of BOC-001 in the photodegradation of MO under UV light.

On the other hand, the indirect dye photosensitization degradation process includes initial photoexcitation of the dye molecules, injection of photoexcited electrons into the conduction band of the semiconductor, and capture of the injected electrons by surface-adsorbed molecular oxygen to generate active species (e.g., $O_2^{-\bullet}$, $OH^{\bullet}$, etc.) for pollutant degradation.[23,24] Unlike the direct semiconductor photoexcitation degradation, the valence band of the semiconductor is not involved in the photoreaction during the indirect dye photosensitization degradation process. Moreover, direct contact between the dye molecules and the semiconductor is a prerequisite for the injection of photoexcited electrons into the conduction band of the semiconductor.[25] Therefore, the photocatalytic performance of the BOC SCNSs in the photosensitization process intimately depends on the surface-related interface properties between the BOC SCNSs and the dye molecules. Obviously, BOC-010 with its larger surface area as well as the open channel characteristic could more easily adsorb MO molecules and provide more contact sites between the photocatalyst and dye molecules, facilitating more efficient

dx.doi.org/10.1021/ja210484t | J. Am. Chem. Soc. 2012, 134, 4473–4476

electron injection from the photoexcited dye into the conduction band of the catalyst, resulting in more MO photodegradation over BOC-010 than BOC-001 during the indirect dye photosensitization process.

To confirm the above analyses, the two kinds of BOC SCNSs were further used to degrade colorless salicylic acid (SA) under UV and visible-light irradiation, respectively. Similar to the case of MO, BOC-001 exhibited higher photoreactivity than BOC-010 for degradation of SA via the direct semiconductor photoexcitation process under UV light (Figures S15 and S16). As the SA cannot be excited by visible light, the indirect dye photosensitization degradation process could not take place. Therefore, we could not observe the degradation of SA over the two kinds of samples under visible-light irradiation (Figure S17). All of these results confirm that the BOC SCNSs with exposed {001} facets favor pollutant degradation under UV light because of their unique surface properties and more suitable internal electric fields, while BOC SCNSs with exposed {010} facets might be powerful for dye degradation under visible light because of their larger surface area and open channel characteristic.

In conclusion, we have synthesized BiOCl single-crystalline nanosheets with exposed {001} and {010} facets via a facile hydrothermal route. The resulting BiOCl single-crystalline nanosheets with exposed {001} facets exhibited higher activity for direct semiconductor photoexcitation pollutant degradation under UV light because of a cooperative effect between the surface atomic structure and suitable internal electric fields. However, the counterpart with exposed {010} facets possessed superior activity for indirect dye photosensitization degradation under visible light because of its larger surface area and open channel characteristic. These findings could shed light on the deep understanding of facet-dependent photoreactivity of semiconductors and the fine manipulation of their photoreactivity as well as the development of new photocatalysts.

■ ASSOCIATED CONTENT

Supporting Information

Experimental details, additional SEM images, XRD patterns, DRS spectra, a nitrogen adsorption−desorption isotherm, PL spectra, additional data, and the possible mechanism of facet-dependent synthesis. This material is available free of charge via the Internet at http://pubs.acs.org.

■ AUTHOR INFORMATION

Corresponding Author

zhanglz@mail.ccnu.edu.cn

Notes

The authors declare no competing financial interest.

■ ACKNOWLEDGMENTS

This work was supported by National Science Foundation of China (Grants 21073069, 91023010, 21177048, and 21103141), the Program for Innovation Team of Hubei Province (Grant 2009CDA048), and the Program for Changjiang Scholars and Innovative Research Team in University (Grant IRT0953).

■ REFERENCES

(1) Kiskinova, M. *Chem. Rev.* **1996**, *96*, 1431.
(2) Somorjai, G. A. *Chem. Rev.* **1996**, *96*, 1223.
(3) Seker, F.; Meeker, K.; Kuech, T. F.; Ellis, A. B. *Chem. Rev.* **2000**, *100*, 2505.
(4) Jiang, Z. Y.; Kuang, Q.; Xie, Z. X.; Zheng, L. S. *Adv. Funct. Mater.* **2010**, *20*, 3634.
(5) Liu, G.; Sun, C. H.; Yang, H. G.; Smith, S. C.; Wang, L. Z.; Lu, G. Q.; Cheng, H. M. *Chem. Commun.* **2010**, *46*, 755.
(6) Fang, W. Q.; Gong, X. Q.; Yang, H. G. *J. Phys. Chem. Lett.* **2011**, *2*, 725.
(7) Liu, G.; Yu, J. C.; Lu, G. Q.; Cheng, H. M. *Chem. Commun.* **2011**, *47*, 6763.
(8) Liu, G.; Wang, L. Z.; Yang, H. G.; Cheng, H. M.; Lu, G. Q. *J. Mater. Chem.* **2010**, *20*, 831.
(9) Liu, S. W.; Yu, J. G.; Jaroniec, M. *J. Am. Chem. Soc.* **2010**, *132*, 11914.
(10) Liu, S. W.; Yu, J. G.; Jaroniec, M. *Chem. Mater.* **2011**, *23*, 4085.
(11) Pan, J.; Liu, G.; Lu, G. Q.; Cheng, H. M. *Angew. Chem., Int. Ed.* **2011**, *50*, 2133.
(12) Bi, Y. P.; Ouyang, S. X.; Umezawa, N.; Cao, J. Y.; Ye, J. H. *J. Am. Chem. Soc.* **2011**, *133*, 6490.
(13) Kuo, C. H.; Yang, Y. C.; Gwo, S.; Huang, M. H. *J. Am. Chem. Soc.* **2011**, *133*, 1052.
(14) Wang, D. G.; Jiang, H. F.; Zong, X.; Xu, Q.; Ma, Y.; Li, G. L.; Li, C. *Chem.—Eur. J.* **2011**, *17*, 1275.
(15) Yang, H. G.; Sun, C. H.; Qiao, S. Z.; Zou, J.; Liu, G.; Smith, S. C.; Cheng, H. M.; Lu, G. Q. *Nature* **2008**, *453*, 638.
(16) Yang, H. G.; Liu, G.; Qiao, S. Z.; Sun, C. H.; Jin, Y. G.; Smith, S. C.; Zou, J.; Cheng, H. M.; Lu, G. Q. *J. Am. Chem. Soc.* **2009**, *131*, 4078.
(17) Liu, G.; Yang, H. G.; Wang, X.; Cheng, L.; Pan, J.; Lu, G. Q.; Cheng, H. M. *J. Am. Chem. Soc.* **2009**, *131*, 12868.
(18) Zhang, K. L.; Liu, C. M.; Huang, F. Q.; Zheng, C.; Wang, W. D. *Appl. Catal., B* **2006**, *68*, 125.
(19) Tang, J. W.; Zou, Z. G.; Ye, J. H. *J. Phys. Chem. B* **2003**, *107*, 14265.
(20) Zhang, K.; Liang, J.; Wang, S.; Liu, J.; Ren, K. X.; Zheng, X.; Luo, H.; Peng, Y. J.; Zou, X.; Bo, X.; Li, J. H.; Yu, X. B. *Cryst. Growth Des.* **2012**, *12*, 793.
(21) Hoffmann, M. R.; Martin, S. T.; Choi, W. D.; Bahnemann, W. *Chem. Rev.* **1995**, *95*, 69.
(22) Linsebigler, A. L.; Lu, G. Q.; Yates, J. T. Jr. *Chem. Rev.* **1995**, *95*, 735.
(23) Zhao, J. C.; Chen, C. C.; Ma, W. H. *Top. Catal.* **2005**, *35*, 269.
(24) Chen, C. C.; Zhao, J. C.; Ma, W. H. *Chem. Soc. Rev.* **2010**, *39*, 4206.
(25) Ge, S. X.; Zhang, L. Z. *Environ. Sci. Technol.* **2011**, *45*, 3027.